2016 14th International Conference on Control, Automation, Robotics & Vision
Phuket, Thailand, 13-15th November 2016 (ICARCV 2016)

A Survey on Tactical Control Algorithms for Path Tracking Unmanned Surface Vehicles

Murat Kumru, Kemal Leblebicioğlu
Department of Electrical and Electronics Engineering,
Middle East Technical University,
Ankara, Turkey.
kumru@metu.edu.tr

İzzet Kağan Erünsal, Kenan Ahıska
ASELSAN Inc.,
Ankara, Turkey.

***Abstract*—In this study, a survey on control allocation algorithms in tactical level control for path tracking unmanned surface vehicles (USV) is conducted. The strategic goal in the path tracking problem is to assist navigation solution of an unmanned underwater vehicle (UUV). USV with the help of its onboard acoustic sensors, tracks UUV according to constant bearing guidance rule. The survey on tactical controllers comprises comparisons of tracking performances of USVs under proportional-integral-derivative, pole placement, feedback linearization and sliding mode controllers according to the strategic goal. The parameters of the controllers are tuned with a common elitist genetic algorithm optimization infrastructure. The disturbance rejection capabilities of the controllers are discussed through Monte Carlo simulations of USVs within various wave disturbances as well.**

***Index Terms*—Unmanned surface vehicles, USV, modeling, PID, pole placement, feedback linearization, sliding mode controller, path tracking, genetic algorithm.**

I. Introduction

Unmanned surface vehicles (USV) are used and proposed when manned vehicles are tried to be avoided due to dangerous characteristics of the mission environment.

Motion control schemes for mechanical systems such as USVs can be treated in a hierarchical scheme consisting of three levels in general [1], [2]. The upper level is called strategic control level where guidance laws are employed to serve kinematic control according to mission objectives. The intermediate level, tactical control level, performs kinetic control and control allocation to fulfill commands from strategic control level. The lower level is execution level where the control commands are realized under constraints of the actuators. The presented modular structure allows optimization of each control level without detailed knowledge of the characteristics of other control levels in the hierarchy. The mission space is mainly divided into four scenarios according to their objectives: point stabilization, trajectory tracking, path following and path maneuvering [3]. Point stabilization can be evaluated as a special case of target tracking as well [2]. The scenarios can be explained as follows:

- *Target tracking*: Without apriori information about target trajectory, i.e., with no information about future position of the target, tracking the motion of a target, either stationary (point stabilization) or in motion.
- *Path following*: Without any restriction on time, following a predefined path.
- *Path tracking*: Following a target moving along a predefined path. This scenario does not require apriori information about the motion of the target. It can be evaluated as a path following problem with restriction on time as well.
- *Path maneuvering*: Gaining information about maneuverability of the vehicle through motions along a predefined path. These scenarios resemble into the gap between path following and path tracking scenarios.

Tactical control problem for USVs has been a critical research area, [4]. The control inputs at tactical level are surge speed and yaw orientation of the vehicle. According to mission objectives, the controller performances are evaluated in terms of the position deviation from the desired route or the final destination point, time or other temporal measures, total energy consumption, transient responses of the closed loop control scheme, or stability of the vehicle throughout its motion. However, establishing a common benchmark environment for comparison of these control algorithms for a defined mission objective has always been an active topic for researchers.

In this study, to provide assistance to navigation of an unmanned underwater vehicle (UUV), a path tracking scenario is defined for a USV. For the path tracking USV, tactical control allocation methods based on classical PID, pole placement, sliding mode and feedback linearization control algorithms are studied and compared. A mathematical vehicle motion model based on robot model [5], is stated. The parameters of the autopilot designs are tuned with a common elitist genetic algorithm infrastructure. As the guidance law, constant bearing algorithm is utilized. The closed loop path tracking performances of the tactical control algorithms based on their total deviation from the position of UUV are compared. The disturbance rejection capabilities of the controllers are discussed by running Monte Carlo simulations under different wave conditions.

II. Mathematical Modeling

A mathematical model accounting for the motion of a surface vessel is constructed to fulfill the need in the design procedure of the control algorithms. The following model

* This research was supported by ASELSAN Inc.

978-1-5090-3549-6/16/$31.00 ©2016 IEEE

having 6 degrees of freedom (DOF) is adopted from [5].

$$\dot{\eta} = \boldsymbol{J}_\Theta(\eta)\boldsymbol{\nu} \tag{1}$$

$$\boldsymbol{M}\dot{\boldsymbol{\nu}} + \boldsymbol{C}(\boldsymbol{\nu})\boldsymbol{\nu} + \boldsymbol{D}(\boldsymbol{\nu})\boldsymbol{\nu} + \boldsymbol{g}(\eta) + \boldsymbol{g}_0 = \tau + \tau_{dist} \tag{2}$$

where $\eta \triangleq [x\ y\ z\ \phi\ \theta\ \psi\ ]^{\mathrm{T}} \in \mathbb{R}^3 \times \mathbb{S}^3$ represents the linear positions and Euler angles; $\boldsymbol{\nu} \triangleq [u\ v\ w\ p\ q\ r]^{\mathrm{T}} \in \mathbb{R}^6$ represents the linear and angular velocities of the body fixed reference frame {b} with respect to the earth fixed reference frame {e}; $\boldsymbol{J}_\Theta(\eta)$ is the transformation matrix

$$\begin{bmatrix} \dot{\boldsymbol{p}}^e_{b|e} \\ \dot{\Theta}_{eb} \end{bmatrix} = \boldsymbol{J}_\Theta(\eta) \begin{bmatrix} \boldsymbol{v}^b_{b|e} \\ \omega^b_{b|e} \end{bmatrix} \tag{3}$$

$$\boldsymbol{J}_\Theta(\eta) = \begin{bmatrix} \boldsymbol{R}^e_b(\Theta_{eb}) & \boldsymbol{0}_{3\times3} \\ \boldsymbol{0}_{3\times3} & \boldsymbol{T}_\Theta(\Theta_{eb}) \end{bmatrix} \tag{4}$$

which transforms the linear and angular velocities ($\boldsymbol{v}^b_{b|e}$, $\omega^b_{b|e}$) resolved in {b} to the linear velocities resolved in {e}, $\dot{\boldsymbol{p}}^e_{b|e}$, and Euler rates, $\dot{\Theta}_{eb}$, by using Euler angle rotation matrix, $\boldsymbol{R}^e_b(\Theta_{eb})$, and angular velocity transformation matrix, $\boldsymbol{T}_\Theta(\Theta_{eb})$. $\boldsymbol{M}$ stands for the system inertial matrix, it is positive definite, symmetric and constant; $\boldsymbol{C}(\boldsymbol{\nu})$ denotes the centrifugal and coriolis matrix, it is skew symmetric; $\boldsymbol{D}(\boldsymbol{\nu})$ refers to the hydrodynamic damping matrix, it is positive definite; the buoyancy forces, $\boldsymbol{g}(\eta)$, and gravitational forces, $\boldsymbol{g}_0$, are together called restoring forces since they essentially attempt to transfer the vehicle to its equilibrium state within the range of stability; τ represents forces and moments produced by vessel fixed thrusters; τ_{dist} symbolizes environmental disturbances due to waves.

A modified Pacific Islander Tugboat is employed as a test platform in this study. Measuring 900 mm in length, 290 mm in width and 260 mm in height, it is a detailed 1/40 scale of the actual vessel. The completely equipped craft consisting of a one-piece fiberglass hull with rubber fenders and tires is illustrated in Fig. 1. There are two independently controllable propellers located at the back of the stern. The vehicle can travel up to 2 m/s using its two electric motors which are powered by a Lithium-polymer (Li-Po) battery. The weight of the boat is about 11 kg including the equipments and a few kilograms of lead shot added for ballast.The parameters of the vehicle motion model in (1) and (2) have been identified in consequence of a comprehensive study, the details of which can be found in [6]. It should be noted that a 6 DOF motion model is preferred in this study to be able to acquire high fidelity model for the simulation and control of a comparably small surface vehicle, [7]. Since disturbance rejection capabilities of the controllers will be investigated, it is necessary to mention characteristics of disturbance forces as well. Considering surface vessels, there are three main types of environmental disturbances: 1. Wind-generated waves, 2. Ocean currents, and 3. Wind forces.

For this study, only wind-generated waves are considered since they are the most dominant disturbance source in test environment. The model representing the effects of waves has three main components and these elements can be found in (5) - (7), [5]. These forces can be directly added to model as surge, sway forces and yaw torques.

$$X_w(t) = \sum_{i=1}^{N} \rho_w g B L T c(\psi - \beta) s_i(t) \tag{5}$$

$$Y_w(t) = \sum_{i=1}^{N} \rho_w g B L T s(\psi - \beta) s_i(t) \tag{6}$$

$$N_w(t) = \sum_{i=1}^{N} \frac{1}{24} \rho_w g B L (L^2 - B^2) s2(\psi - \beta) s_i^2(t) \tag{7}$$

Here L, B and D are the length, beam and draft of the wetted part of the surface vessel, respectively. g_w is the density of water, $s_i(t)$ is the wave slope and $\psi - \beta$ is the angle between ship heading and wave direction. The wave slope $s_i(t)$ can be found by using specific wave spectral density function $S(w_i)$. In this study, Pierson-Moskowitz spectrum, [5], is used. The expression of this spectrum is given in (8).

$$S(w) = 8.1 \times 10^{-3} g^2 exp(-\frac{3.11}{H_s^2} w^{-4}) \tag{8}$$

where g is the gravitational constant and H_s is the significant wave height (mean of the one-third of the highest wave).

III. Tactical Level Controller Designs

A. PID Based Controller

As a first alternative to autopilot design, PID based controller whose structure is given by (9) is utilized.

$$G_c(s) = K_p + \frac{K_i}{s} + \frac{K_d s}{T_f s + 1} \tag{9}$$

Since the objective is to control the surge speed and yaw position of the vehicle by generating left and right thruster forces, the control system is multiple-input, multiple-output (MIMO). This structure, [6], is depicted in Fig. 2 where the outputs of controllers are weighted and summed to generate thruster commands.

It should be noted that the controller structure is symmetrical, in other words, PID controller couple that generate force output for the left thruster are same as the one for the right thrusters. As a result, PID-1 and PID-2 have same P, I, D and

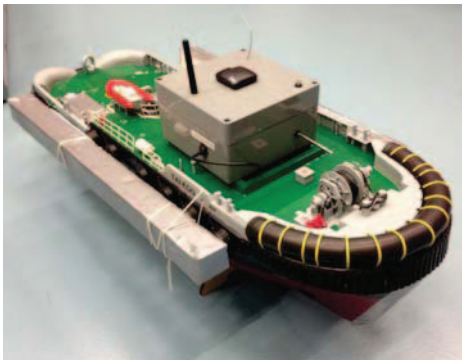

Fig. 1. Model Pacific Islander Tugboat with the installed equipments

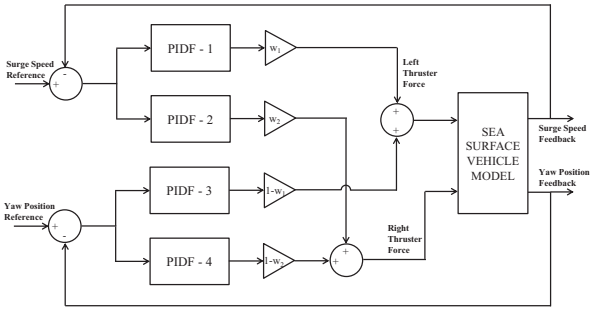

Fig. 2. PID based controller structure

gain parameters, likewise, PID-3 and PID-4 share the same parameters with opposite signs to assure proper and balanced yaw rotations with two thrusters. This approach reduces the number of parameters to be tuned as well.

B. Pole Placement (PP) Based Controller

Another controller employed at the tactical level is based on pole placement theory. The primary objective of this controller design is to find an appropriate linear state feedback gain, denoted by $\boldsymbol{K}$ in (10), to obtain desired performance.

$$\boldsymbol{u}(t) = -\boldsymbol{K}\boldsymbol{x}(t) \tag{10}$$

At this stage, it should be noted that the system is not completely controllable. As a result, PP controller is designed for controllable subspace of the system representation to place the poles of the system at desired locations.

Within the scope of this study, the control algorithm is supposed to track reference signals which are not necessarily zero. To apply the PP controller on this tracking problem, the state vector is augmented by the integral of errors between the reference signal, $\boldsymbol{r}(t)$ and the outputs to be controlled, [5]. The original system is represented by (11) and (12).

$$\dot{\boldsymbol{x}} = \boldsymbol{A}\boldsymbol{x} + \boldsymbol{B}\boldsymbol{u} \tag{11}$$

$$\boldsymbol{y} = \boldsymbol{C}\boldsymbol{x} \tag{12}$$

The state vector is augmented with $\boldsymbol{z}$ whose characteristics are given in (13). Thereby, the differential equations of the system are rewritten in (14),

$$\dot{\boldsymbol{z}} = \boldsymbol{r}(t) - \boldsymbol{y} = \boldsymbol{r}(t) - \boldsymbol{C}\boldsymbol{x}. \tag{13}$$

$$\dot{\boldsymbol{x}}_{aug} = \begin{bmatrix} \dot{\boldsymbol{x}} \\ \dot{\boldsymbol{z}} \end{bmatrix} = \boldsymbol{A}_{aug} \begin{bmatrix} \boldsymbol{x} \\ \boldsymbol{z} \end{bmatrix} + \boldsymbol{B}_{aug}\boldsymbol{u} + \begin{bmatrix} \boldsymbol{0} \\ \boldsymbol{I} \end{bmatrix} \boldsymbol{r} \tag{14}$$

where

$$\boldsymbol{A}_{aug} \triangleq \begin{bmatrix} \boldsymbol{A} & \boldsymbol{0} \\ -\boldsymbol{C} & \boldsymbol{0} \end{bmatrix}, \quad \boldsymbol{B}_{aug} \triangleq \begin{bmatrix} \boldsymbol{B} \\ \boldsymbol{0} \end{bmatrix}. \tag{15}$$

Let the desired values of the states and the inputs are symbolized by $\boldsymbol{x}_{aug,d}$ and $\boldsymbol{u}_d$, respectively. The desired values are subtracted from the instantaneous state values while $\boldsymbol{r}(t)$ is assumed to be constant, i.e., $\boldsymbol{r}(t) = \boldsymbol{r}\ \forall\ t$.

$$\dot{\boldsymbol{x}}_{aug} - \dot{\boldsymbol{x}}_{aug,d} = \boldsymbol{A}_{aug} \begin{bmatrix} \boldsymbol{x} - \boldsymbol{x}_d \\ z - z_d \end{bmatrix} + \boldsymbol{B}_{aug}(\boldsymbol{u} - \boldsymbol{u}_d) \tag{16}$$

The state error vector, $\boldsymbol{e}$, and the input error vector, $\boldsymbol{v}$, are defined as in (17). The notation in (16) is simplified leading to (18).

$$\boldsymbol{e} = \boldsymbol{x}_{aug} - \boldsymbol{x}_{aug,d}, \quad \boldsymbol{v} = \boldsymbol{u} - \boldsymbol{u}_d \tag{17}$$

$$\dot{\boldsymbol{e}} = \boldsymbol{A}_{aug}\boldsymbol{e} + \boldsymbol{B}_{aug}\boldsymbol{v} \tag{18}$$

In the end, the tracking problem is transformed into a regulation one in (18). The control law, $\boldsymbol{v}$, for the above problem is to be identified by determining the gain vector, $\boldsymbol{K}_{aug}$, in (19). Note that $\boldsymbol{K}_{aug}$ can be partitioned as in (20).

$$\boldsymbol{v} = -\boldsymbol{K}_{aug}\boldsymbol{e} \tag{19}$$

$$\boldsymbol{K}_{aug} = \begin{bmatrix} \boldsymbol{K}_1 & \boldsymbol{K}_2 \end{bmatrix} \tag{20}$$

Thus, the following control law is obtained while $\boldsymbol{u}_d$ and $\boldsymbol{z}_d$ are assumed to be zero.

$$\boldsymbol{u} = -\boldsymbol{K}_1(\boldsymbol{x} - \boldsymbol{x}_d) - \boldsymbol{K}_2\boldsymbol{z} \tag{21}$$

C. Feedback Linearization (FL) Based Controller

Feedback linearization technique is essentially employed to render the relation between the input and output of the system linear without appealing Jacobian linearization. It is realized by the selection of a control law which is a nonlinear mapping of the state feedback, [8]. The output of the system is selected as in (22).Note that (1) and (2) can be manipulated to express the dynamics of the system in the form of (23).

$$\boldsymbol{y} = \begin{bmatrix} \psi & u \end{bmatrix}^{\mathrm{T}} \tag{22}$$

$$\begin{bmatrix} \dot{\eta} \\ \dot{\boldsymbol{\nu}} \end{bmatrix} = \begin{bmatrix} \boldsymbol{J}_{\Theta}(\eta)\boldsymbol{\nu} \\ \boldsymbol{M}^{-1}\left[\tau_d + \tau_g + \tau_a + \tau_c - \boldsymbol{C}(\boldsymbol{\nu})\boldsymbol{\nu}\right] \end{bmatrix} + \begin{bmatrix} 0 \\ \boldsymbol{M}^{-1}\tau_t \end{bmatrix} \tag{23}$$

$\boldsymbol{M}^{-1}\tau_t$ is a linear function of the forces and moments generated by the thrusters and can be formulated as

$$\boldsymbol{M}^{-1}\tau_t = \boldsymbol{G}_t\boldsymbol{u} \tag{24}$$

where $\boldsymbol{G}_t \in \mathbb{R}^{6\times 2}$, and $\boldsymbol{u} \in \mathbb{R}^{2\times 1}$ is the input vector whose elements are the forces exerted onto the body by left and right thrusters.Subsequently, (23) takes the following form:

$$\begin{bmatrix} \dot{\eta} \\ \dot{\boldsymbol{\nu}} \end{bmatrix} = \begin{bmatrix} \boldsymbol{J}_{\Theta}(\eta)\boldsymbol{\nu} \\ \boldsymbol{M}^{-1}\left[\tau_d + \tau_g + \tau_a + \tau_c - \boldsymbol{C}(\boldsymbol{\nu})\boldsymbol{\nu}\right] \end{bmatrix} + \boldsymbol{G}\boldsymbol{u} \tag{25}$$

where $\boldsymbol{G} \triangleq \begin{bmatrix} \boldsymbol{0} \\ \boldsymbol{G}_t \end{bmatrix} \in \mathbb{R}^{12\times 2}$, and $\boldsymbol{G}$ can be rewritten as

$$\boldsymbol{G} = \begin{bmatrix} \boldsymbol{g}_1 & \boldsymbol{g}_2 \end{bmatrix} \tag{26}$$

where $\boldsymbol{g}_1$ and $\boldsymbol{g}_2$ are the first and second columns of $\boldsymbol{G}$, respectively. Finally, the system is represented by (27).

$$\dot{\boldsymbol{x}} = f(\boldsymbol{x}) + g(\boldsymbol{x})\boldsymbol{u} \tag{27}$$

$$f(\boldsymbol{x}) = \begin{bmatrix} \boldsymbol{J}_{\Theta}(\eta)\boldsymbol{\nu} \\ \boldsymbol{M}^{-1}\left[\tau + \tau_{dist} - \boldsymbol{C}(\boldsymbol{\nu})\boldsymbol{\nu} - \boldsymbol{D}(\boldsymbol{\nu})\boldsymbol{\nu} - \boldsymbol{g}(\eta) - \boldsymbol{g}_0\right] \end{bmatrix}$$

$$g(\boldsymbol{x}) = \boldsymbol{G}$$

The implementation of the FL controller is based on the representation given in (27). The following observations are made by considering Lie derivatives of the outputs, [9].

1) $L_{g_1}\psi \equiv 0$, $L_{g_2}\psi \equiv 0$ meaning that the input vector does not appear in the first derivative of ψ,
2) $L_{g_1}L_f\psi \neq 0$, $L_{g_2}L_f\psi \neq 0$,
3) $L_{g_1}L_f u \neq 0$, $L_{g_2}L_f u \neq 0$,

In other words, the relative degrees of ψ and u are found to be 2 and 1, respectively. Finally, the following equations regarding the output variables can be written, [10].

$$\begin{bmatrix} \ddot{\psi} \\ \dot{u} \end{bmatrix} = \begin{bmatrix} L_f^2\psi \\ L_f u \end{bmatrix} + \boldsymbol{A}(\boldsymbol{x})\boldsymbol{u} \tag{28}$$

$$\boldsymbol{A}(\boldsymbol{x}) = \begin{bmatrix} L_{g_1}L_f\psi & L_{g_2}L_f\psi \\ L_{g_1}u & L_{g_2}u \end{bmatrix} \tag{29}$$

The control law is then selected as in (30) which brings about the input-output relationship in (31). A PP controller will be employed to control this linear system.

$$\boldsymbol{u} = -\boldsymbol{A}^{-1}(\boldsymbol{x}) \begin{bmatrix} L_f^2\psi \\ L_f u \end{bmatrix} + \boldsymbol{A}^{-1}(\boldsymbol{x})\boldsymbol{v} \tag{30}$$

$$\begin{bmatrix} \ddot{\psi} \\ \dot{u} \end{bmatrix} = \begin{bmatrix} v_1 \\ v_2 \end{bmatrix} \tag{31}$$

D. Sliding Mode Controller (SMC)

Sliding mode control with its performance being insensitive to disturbances in plant and environment is considered as a robust control technique. In order to implement SMC effectively, USV model is decoupled into propulsion and heading subsystems, and actuation inputs are arranged accordingly. The selection of states separates the dominant dynamics of the propulsion and heading from those insignificant, [11]. The propulsion subsystem includes only the surge speed in $\{\mathrm{b}\}$ frame while the heading subsystem includes sway and yaw speeds in $\{\mathrm{b}\}$ frame and yaw position in $\{\mathrm{e}\}$ frame. Decoupled system equations for propulsion and heading subsystems are given in (32) and (33).

$$\dot{u} = A_p u + B_p \tau_1 + f(u) \tag{32}$$

$$\begin{bmatrix} \dot{v} & \dot{r} & \dot{\psi} \end{bmatrix}^T = \boldsymbol{A_h} \begin{bmatrix} v & r & \psi \end{bmatrix}^T + B_h \tau_3 + f(v, r, \psi) \tag{33}$$

where u, v, r and ψ are the states, $A_p, \boldsymbol{A_h}, B_p$ and B_h are the system and input matrices, τ_1 is the surge force, τ_3 is the yaw torque and $f(\cdot)$s are functions that describe any difference that would cause the system to deviate from its equilibrium point such as nonlinearities, unmodeled dynamics and external disturbances, [11]. SMC consists of a nominal part (equivalent term) that provides main control action and an additional term (switching term) dealing with the disturbances and unmodeled dynamics, [12].

$$u_{SM} = u_{eq} + u_{sw} \tag{34}$$

For this study, the equivalent component of the control action is selected as state space feedback gain controller for reference tracking as in (35).

$$u_{eq} = \boldsymbol{K_f x_d} - \boldsymbol{k}^{\mathrm{T}}\boldsymbol{x} \tag{35}$$

where $\boldsymbol{k}$ is the feedback gain according to robust Pole Placement Theory proposed by [13]. The switching term is a nonlinear term and provides additional control action. The general form of switching term is given in (36), [11].

$$u_{sw} = (\boldsymbol{h}^{\mathrm{T}}\boldsymbol{b})^{-1}(\boldsymbol{h}^{\mathrm{T}}\dot{\boldsymbol{x}}_{\boldsymbol{d}} - \eta sgn(\boldsymbol{\sigma}(\hat{\boldsymbol{x}}))) \tag{36}$$

where $\boldsymbol{h}$ is the right eigen-vector (corresponds to zero eigenvalue) of the desired closed loop system matrix, $\boldsymbol{A_c}$, $\boldsymbol{b}$ is the input matrix, $\dot{\boldsymbol{x}}_{\boldsymbol{d}}$ is the derivative of the desired system vector, η is the switching gain which determines the amplitude of the additional switching action, $\boldsymbol{\sigma}(\hat{\boldsymbol{x}})$ is the sliding surface as a function of tracking error $\hat{\boldsymbol{x}}$. The sliding surface utilized in this work can be expressed as (37), where $\boldsymbol{x}$ is the states and $\boldsymbol{x_d}$ is the desired states.

$$\boldsymbol{\sigma}(\hat{\boldsymbol{x}}) = \boldsymbol{h}^{\mathrm{T}}\hat{\boldsymbol{x}} = \boldsymbol{h}^{\mathrm{T}}(\boldsymbol{x} - \boldsymbol{x_d}) \tag{37}$$

Chattering along the sliding surface, a function of thickness parameter, Φ, is softened by replacing sgn function with $tanh$. As a result, final form of the control laws can be constructed as in (38) and (39), where subscripts p and h correspond to propulsion and heading subsystems, respectively.

$$\tau_1 = K_{fp}u_d - \boldsymbol{k_p}^{\mathrm{T}}u + (\boldsymbol{h_p}^{\mathrm{T}}\boldsymbol{B_p})^{-1}\left(\boldsymbol{h_p}^{\mathrm{T}}\dot{\boldsymbol{u}}_{\boldsymbol{d}} - \eta_p tanh\left(\frac{\boldsymbol{\sigma_p}(u - u_d)}{\Phi_p}\right)\right) \tag{38}$$

$$\tau_3 = \boldsymbol{K_{fh}x_d} - \boldsymbol{k_h}^{\mathrm{T}}\boldsymbol{x_h} + (\boldsymbol{h_h}^{\mathrm{T}}\boldsymbol{B_h})^{-1}\left(\boldsymbol{h_h}^{\mathrm{T}}\dot{\boldsymbol{x}}_{\boldsymbol{hd}} - \eta_h tanh\left(\frac{\boldsymbol{\sigma_h}(\boldsymbol{x_h} - \boldsymbol{x_{hd}})}{\Phi_h}\right)\right) \tag{39}$$

IV. Method

A. Genetic Algorithm to Tune Autopilot Parameters

Genetic algorithm (GA) is an evolutionary optimization algorithm that can be utilized to solve optimization problems with non-smooth, highly non-linear and stochastic nature. Basic principle is the natural selection inspired from biological evolution. At each step known as generations, GA creates a population based on selection, crossover and mutation rules. Selection rules choose individuals named as parents that contribute to the population at next step. Crossover rules determine the procedure for combining two parents to create an offspring. Mutation rules perform random changes in individuals in order to increase the population diversity.

In this study, '*ga*' built-in function in the 'Global Optimization Toolbox' of MATLAB is employed due to its flexible interface. The cost function is constructed to take yaw position and surge speed errors into account.

B. Constant Bearing Guidance Law

The strategic goal in the problem is defined as following a UUV and keeping USV on sea surface just above. Since USV tracks a UUV following a predefined path, the problem corresponds to path tracking. In this study, constant bearing (CB), or parallel navigation is implemented for a so-called planar collision geometry with UUV being target and USV

being interceptor. The planar positions of the vehicle and the target which are both resolved in $\{e\}$ are respectively denoted by $\mathbf{p}(t) = [x(t)\ y(t)]^{\mathrm{T}}$, $\mathbf{p}_{\mathrm{t}}(t) = [x_{\mathrm{t}}(t)\ y_{\mathrm{t}}(t)]^{\mathrm{T}} \in \mathbb{R}^2$. Moreover, the linear velocities of the vehicle and the target with respect to $\{e\}$ frame are defined as $\mathbf{v}(t) \triangleq d\mathbf{p}(t)/dt \triangleq \dot{\mathbf{p}}(t)$ and $\mathbf{v}_{\mathrm{t}}(t) \triangleq \dot{\mathbf{p}}_{\mathrm{t}}(t) \in \mathbb{R}^2$. The CB guidance law is given as

$$\mathbf{v}_{\mathrm{d}}(t) = \mathbf{v}_{\mathrm{t}}(t) + \mathbf{v}_{\mathrm{a}}(t) \tag{40}$$

where $\mathbf{v}_{\mathrm{d}}(t)$ is the desired velocity to be fed to the tactical controllers as the reference signal; $\mathbf{v}_{\mathrm{t}}(t)$ is the instantaneous velocity of the target and $\mathbf{v}_{\mathrm{a}}(t)$ is the velocity vector along which the vehicle will travel to intercept the target. $\mathbf{v}_{\mathrm{a}}(t)$ is selected as

$$\mathbf{v}_{\mathrm{a}}(t) = \kappa(t)\frac{\tilde{\mathbf{p}}(t)}{|\tilde{\mathbf{p}}(t)| + \epsilon} \tag{41}$$

where $\tilde{\mathbf{p}}(t) \triangleq \mathbf{p}_{\mathrm{t}}(t) - \mathbf{p}(t)$ is the position error vector and $|\tilde{\mathbf{p}}(t)| = \sqrt{\tilde{\mathbf{p}}(t)^{\mathrm{T}}\tilde{\mathbf{p}}(t)}$ is the Euclidean length of this vector; ϵ is a small constant to prevent division by zero, and $\kappa(t)$ is calculated by

$$\kappa(t) = U_{\mathrm{a,max}}(t)\frac{\tilde{\mathbf{p}}(t)}{\sqrt{|\tilde{\mathbf{p}}(t)|^2 + \triangle_{\tilde{\mathbf{p}}}^2}} \tag{42}$$

where $U_{\mathrm{a,max}}(t) > 0$ is the maximum allowed approach speed and $\triangle_{\tilde{\mathbf{p}}} > 0$ is utilized to dwindle down the approach speed to obtain desired transient response while the vehicle is closing up to the rendezvous point. Subsequently, $\mathbf{v}_{\mathrm{d}}(t)$ is represented in polar coordinates to obtain corresponding yaw angle, $\psi_d(t)$, and surge speed, $u_d(t)$, commands to be tracked.

V. Results

A. Path Tracking Performances

The tracking results together with the reference path are presented in Fig. 3. Results show that GA optimization yields to controller parameters accomplishing satisfactory path tracking performances for all cases. The average position deviation from the path to be tracked for PID, PP, FL and SMC are $(2.96, 2.42, 2.47, 5.88) \times 10^{-2}\ m$, respectively. Furthermore, the pitch and roll angles are observed to be bounded throughout all simulations. In Fig. 4, position errors for all controllers are presented. The results demonstrate that while straight line performances of all controllers are similar, maneuvering characteristics exhibit some differences. In maneuvering, USV controlled with SMC deviates from the curved path more compared to the ones with other controllers. The reasons behind this result are decoupling of states in model utilized by SMC and the complexity of heading subsystem. Furthermore, USV with PID controller exhibits oscillatory behavior along straight line sections. In other controllers either the plant model is considered or the sway speed errors are taken into account; however, in PID controller, direct use of position error lacks these information and results in this oscillatory behavior. Furthermore, note that GA optimizes parameters considering only surge speed and yaw position errors, as a result, large gains for PID controller are possible which may lead to oscillations.

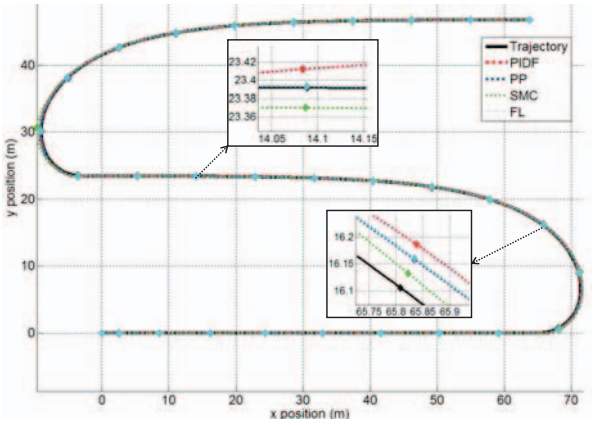

Fig. 3. Path tracking performances of the controllers

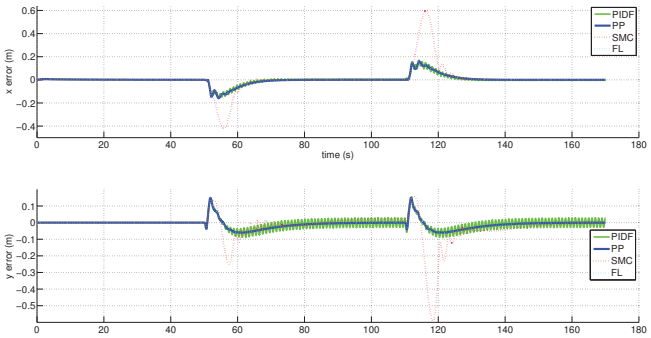

Fig. 4. Errors of the routes in x and y directions

The path tracking performances of the vehicles with different controllers also depend on the guidance law. CB guidance benefits only from the current position of the target, and does not make use of its previous or future positions. Moreover, the orientation information of the target is not considered. Therefore, delays in tracking are inevitable as illustrated in Fig. 3.

B. Disturbance Rejection Performances

The performances of the controllers are compared in terms of their disturbance rejection capabilities through Monte Carlo (MC) simulations as well. The parameters of MC simulations are direction and height of the wave. The vehicle is perturbed with possible combinations of the spanned ranges: 0-360 degrees for direction and 0-0.07 meter for the height. The results are presented in Fig. 5-8.

It is observed that with increasing wave height, deviations from the desired path increase as expected. Moreover, it is found that tracking performance degrades when waves are misaligned with vehicle major axis throughout its motion (45, 135, 225, 315 degrees). The reduction in the performance is due to lack of inputs to compensate the side wave disturbances.

The results present that USVs with PID, FL and PP controllers show similar satisfying performances under disturbances. It can be stated that these results are due to direct utilization of the model of the vessel for FL and high gains

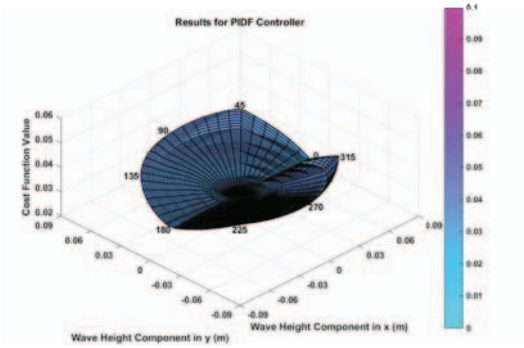

Fig. 5. Disturbance rejection performance of PID

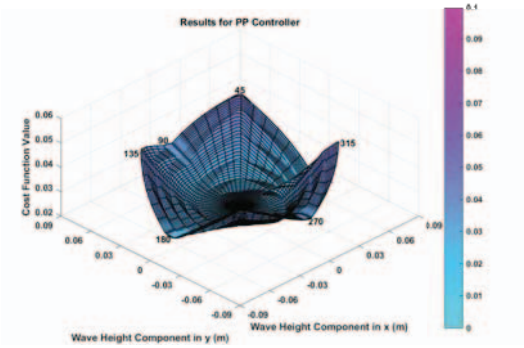

Fig. 6. Disturbance rejection performance of PP

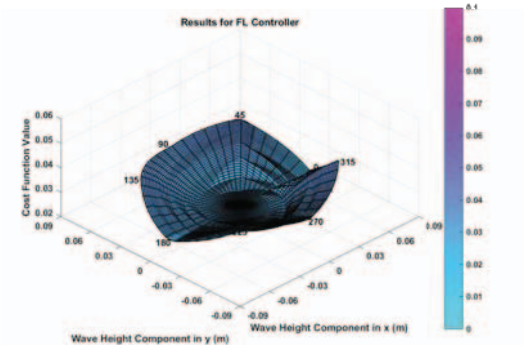

Fig. 7. Disturbance rejection performance of FL

associated with PP and PID. On the other hand, SMC has the worst disturbance rejection capability due to decoupling of states and complexity of heading subsystem.

VI. Conclusion

In this study, autopilot designs for a USV with perfect tracking sensors which is employed to assist a UUV for its navigation solution are discussed. Since USV tracks a UUV following a predefined path, the problem corresponds to path tracking. The study focuses on performances of various tactical level controllers tuned with a common elitist GA. Under various wave disturbances, controller performances are simulated and compared. It is observed that all controllers with CB guidance law yield to satisfactory results.

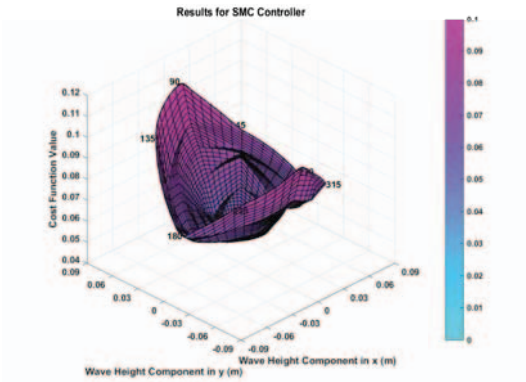

Fig. 8. Disturbance rejection performance of SMC

In the near future, experimental validation of the controller performances will be performed. Different guidance techniques and sensor model integration techniques will be tested within these experiments. System identification studies will be incorporated with these experiments as well.

References

[1] T. A. Johansen and T. I. Fossen, "Control allocation : A survey," *Automatica*, vol. 49, no. 5, pp. 1087–1103, 2013.

[2] M. Breivik, V. E. Hovstein, and T. I. Fossen, "Straight-line target tracking for unmanned surface vehicles," *Modeling, Identification and Control*, vol. 29, no. 4, pp. 131–149, 2008.

[3] M. Bibuli, M. Caccia, L. Lapierre, and G. Bruzzone, "Guidance of unmanned surface vehicles: Experiments in vehicle following," *IEEE Robotics Automation Magazine*, vol. 19, no. 3, pp. 92–102, Sept 2012.

[4] M. Azzeri, F. Adnan, and M. Zain, "Review of course keeping control system for unmanned surface vehicle," *Jurnal Teknologi*, vol. 74, no. 5, pp. 11–20, 2015.

[5] T. I. Fossen, *Handbook of Marine Craft Hydrodynamics and Motion Control*. John Wiley & Sons, Ltd, 2011.

[6] I. K. Erunsal, "System identification and control of a sea surface vehicle," Master's thesis, Dept. Elec. and Electronics Eng., Middle East Technical Uni., Turkey, 2015.

[7] C. R. Sonnenburg and C. A. Woolsey, "Modeling, identification, and control of an unmanned surface vehicle," *Journal of Field Robotics*, vol. 30, no. 3, pp. 371–398, 2013.

[8] S. Sastry, *Nonlinear Systems: Analysis, Stability, and Control*. Springer-Verlag, New York, 1999.

[9] M. Kumru, "Navigation and control of an unmanned sea surface vehicle," Master's thesis, Dept. Elec. and Electronics Eng., Middle East Technical Uni., Turkey, 2015.

[10] J.-J. E. Slotine and W. Li, *Applied nonlinear control*. NJ: Prantice-Hall, Englewood Cliffs, 1991.

[11] E. W. McGookin, "Optimisation of sliding mode controllers for marine applications: A study of methods and implementation issues," Ph.D. dissertation, Dept. Elec. and Electronics Eng., Uni. of Glasgow, UK, 1997.

[12] E. Alfaro-Cid, E. McGookin, D. Murray-Smith, and T. Fossen, "Genetic algorithms optimisation of decoupled sliding mode controllers: simulated and real results," *Control Engineering Practice*, vol. 13, no. 6, pp. 739–748, 2005.

[13] J. Kautsky, N. K. Nichols, and P. V. Dooren, "Robust pole assignment in linear state feedback," *International Journal of Control*, vol. 41, no. 5, pp. 1129–1155, 1985.